



This open access document is posted as a preprint in the Beilstein Archives at <https://doi.org/10.3762/bxiv.2022.30.v1> and is considered to be an early communication for feedback before peer review. Before citing this document, please check if a final, peer-reviewed version has been published.

This document is not formatted, has not undergone copyediting or typesetting, and may contain errors, unsubstantiated scientific claims or preliminary data.

**Preprint Title** Rapid Fabrication of MgO@g-C<sub>3</sub>N<sub>4</sub> Heterojunction for Photocatalytic Nitric Oxide degradation under Visible Light

**Authors** Minh-Thuan Pham, Duyen P. H. Tran, Xuan-Thanh Bui and Sheng-Jie You

**Publication Date** 27 Apr. 2022

**Article Type** Full Research Paper

**Supporting Information File 1** Supplementary Information.docx; 882.2 KB

**ORCID® iDs** Minh-Thuan Pham - <https://orcid.org/0000-0002-6069-445X>; Duyen P. H. Tran - <https://orcid.org/0000-0003-3152-7270>; Xuan-Thanh Bui - <https://orcid.org/0000-0003-1413-4985>; Sheng-Jie You - <https://orcid.org/0000-0003-0532-9916>

License and Terms: This document is copyright 2022 the Author(s); licensee Beilstein-Institut.

This is an open access work under the terms of the Creative Commons Attribution License (<https://creativecommons.org/licenses/by/4.0>). Please note that the reuse, redistribution and reproduction in particular requires that the author(s) and source are credited and that individual graphics may be subject to special legal provisions.

The license is subject to the Beilstein Archives terms and conditions: <https://www.beilstein-archives.org/xiv/terms>.

The definitive version of this work can be found at <https://doi.org/10.3762/bxiv.2022.30.v1>

# Rapid Fabrication of MgO@g-C<sub>3</sub>N<sub>4</sub> Heterojunction for Photocatalytic Nitric Oxide degradation under Visible Light

Minh-Thuan Pham<sup>1,2,3,‡</sup>, Duyen P.H Tran<sup>2,3, ‡</sup>, Xuan-Thanh Bui<sup>4</sup>, Sheng-Jie You<sup>2,3,\*</sup>

<sup>1</sup>Department of Civil Engineering, Chung Yuan Christian University, Taoyuan 32023, Taiwan

<sup>2</sup>Department of Environmental Engineering, Chung Yuan Christian University, Taoyuan 32023, Taiwan

<sup>3</sup>Center for Environmental Risk Management, Chung Yuan Christian University, Taoyuan 32023, Taiwan

<sup>4</sup>Faculty of Environment and Natural Resources, Ho Chi Minh City University of Technology (HCMUT), VNU-HCM, 268 Ly Thuong Kiet street, District 10, Ho Chi Minh City 700000, Viet Nam

Email: Sheng-Jie You - [sjyou@cycu.edu.tw](mailto:sjyou@cycu.edu.tw)

‡ These authors contributed equally

\* Corresponding author: Sheng-Jie You

## Abstract

Nitric Oxide (NO) is one of air pollutant that is responsible for its impacts in various environmental matrices, human health and other biota. Apart from various technology to treat NO pollution, photocatalytic oxidation process (PCO) under visible light is

considered as an effective process to achieve the feat. This study uses PCO to degrade NO under visible light with the help of photocatalyst. Herein, the MgO@g-C<sub>3</sub>N<sub>4</sub> heterojunctions are synthesized by one-step pyrolysis of MgO and Urea commercial at 550 °C for 2 h. By this way, the photocatalytic NO degradation performance is significantly increased under visible light irradiation. In detail, the photocatalytic efficiency of the MgO@g-C<sub>3</sub>N<sub>4</sub> composites reaches 75.4% with 1.2-fold that of pure g-C<sub>3</sub>N<sub>4</sub> and 4.5-fold that of commercial MgO. Furthermore, the characterizations of the materials are determined by X-ray diffraction (XRD), Fourier transforms infrared spectroscopy (FTIR), and X-ray photoelectron spectroscopy (XPS). The morphology of the materials is determined by scanning electron microscopy (SEM) and transmission electron microscopy (TEM). DRS determines the optical properties and bandgap of the materials. The bandgap of the materials decreases with the increasing amount of the MgO. Besides, the NO conversion, DeNO<sub>x</sub> index, apparent quantum efficiency (AQE), the trapping test, and electron spin resonance (ESR) are invested to understand the photocatalytic mechanism of the materials. The high reusability of the MgO@g-C<sub>3</sub>N<sub>4</sub> composites is determined by 5 times recycling test.

## **Keywords**

MgO, g-C<sub>3</sub>N<sub>4</sub>; photocatalyst; Nitric Oxide; Visible light.

## **Introduction**

Recently, the rapid development of industrialization has been continuously increasing the demand for fossil fuel combustion which leads to a large number of nitrogen oxides emissions. This particular type of air pollutant is responsible for various impacts

ranging from environment disruption (smog, acid rain, etc.) to health problems (COPD, cardiovascular disease, and other) [1–3]. Thus, many researchers have been trying to overcome the problem by applying different kind of treatment technologies. Presently, various approaches have been done to mitigate NO pollution, including catalytic/ non-catalytic [4], oxidation [5], bioprocesses [6], adsorption [7], , absorption [8] and non-thermal plasma technology [9]. Among these, photocatalytic oxidation (PCO) is regarded to be a promising approach for air purification due to its ability in degrading various air pollutants with the presence of light under ambient conditions [10].

Due to its unique properties complied with high chemical stability and low synthesis cost, graphitic carbon nitride has attracted considerable attention in the realm of environmental remediation [11–13]. It is a kind of organic semiconductor, and it effectively absorbs visible light due to its narrow frequency band (<2.7 eV). Based on that reason, it has been consistently regarded as a catalysts with excellent optical property [14, 15]. Unfortunately, its narrow bandgap leads to rapid recombination of electron and hole pairs, and the valence band potential of g-C<sub>3</sub>N<sub>4</sub> (+1.75 eV) is more negative than that of H<sub>2</sub>O/•OH (+2.40 eV), reducing the photocatalytic efficiency [16, 17]. As a well-known approach for overcoming this problem and increasing the lifespan of photo-generated electron (e<sup>-</sup>) – hole (h<sup>+</sup>) pairs in order to achieve increased photocatalytic performance, coupling two semiconductors with optimal band alignment is used to achieve this goal.

MgO is considered as an alkaline metal oxide which possesses a wide bandgap (5 - 3.5 eV), availability, non-toxic and low cost [18, 19]. High band gap energy hinders MgO ability to harvest more visible light, thus lowering photocatalytic performance [20]. Thus, a various of approaches have been taken to enhance the visible light absorption region, particular in coupling with another semiconductor such as g-C<sub>3</sub>N<sub>4</sub>

[21–23], ZnO [24, 25], TiO<sub>2</sub> [26, 27], etc. Among these, the incorporation of MgO and g-C<sub>3</sub>N<sub>4</sub> with the lower bandgap is attributed to be an efficient process for improving photocatalytic process. Li and co-workers reported that the improvement in the photocatalytic efficiency of MgO@g-C<sub>3</sub>N<sub>4</sub> for CO<sub>2</sub> photoreduction under visible light [22]. Similarly, MgO modified g-C<sub>3</sub>N<sub>4</sub> nanostructure enhanced NO<sub>2</sub> removal efficiency [12]. However, the commercial application of MgO as a co-catalyst together with g-C<sub>3</sub>N<sub>4</sub> has not been researched for the photocatalytic NO degradation.

In this study, the combination of MgO and g-C<sub>3</sub>N<sub>4</sub> was performed to form a heterostructure that potentially enhances the visible light absorption efficiency, and thus improves the photocatalysis efficiency. To the best of our knowledge, the one-step synthesis of MgO@g-C<sub>3</sub>N<sub>4</sub> heterojunction composite by one-step pyrolysis method is first studied and applied to NO gas treatment under visible light irradiation. The obtained results in this study may offer the potential for the production of photocatalysts with high efficiency, low cost and ease of large-scale application.

## **Experimental**

### **Synthesis of MgO/g-C<sub>3</sub>N<sub>4</sub>**

For the synthesis of g-C<sub>3</sub>N<sub>4</sub>, 30 g of Urea is ground by manual for 30 min and then placed in a 100 mL crucible. Then, the sample is annealed at 550 °C for 2 h. Next, the obtained sample is naturally cooled down at room temperature, named as g-C<sub>3</sub>N<sub>4</sub>.

For MgO@g-C<sub>3</sub>N<sub>4</sub> composites preparation, both MgO and g-C<sub>3</sub>N<sub>4</sub> are mixed, ground and placed in a 100 mL crucible then annealed at 550 °C for 2 h (Figure 1). Then the sample is cooled down at room temperature naturally. Different mass ratios of MgO

and g-C<sub>3</sub>N<sub>4</sub> are implemented, i.e. 1%, 3% and 5%, named as x-MgO@g-C<sub>3</sub>N<sub>4</sub> (x = 1, 3 and 5%).

## **Characterization**

To evaluate the morphology, physical, chemical, and optical properties of the materials, a variety of analytical techniques have been employed. Scanning electron microscopy (SEM) and high-resolution transmission electron microscopy (HR-TEM) are used to assess the morphology of the material. The crystal phase of material is determined by X-ray diffraction (XRD) with the measurement range of 10° – 80°. Fourier transform infrared spectroscopy (FTIR) is used to determine the chemical bond composition of the materials. Differential reflectance spectroscopy (DRS) determines the change in the bandgap of the material. The elements of this composite are identified by high-resolution X-ray photoelectron spectroscopy (HR-XPS). Finally, the photocatalytic mechanism is determined through trapping tests and electron spin resonance (ESR).

## **Photocatalytic performance**

The photocatalytic activity of as-prepared MgO@g-C<sub>3</sub>N<sub>4</sub> is evaluated by monitoring NO degradation through photocatalytic system. The photocatalytic degradation experiments are performed using a 1.5 L reaction chamber and a Xenon lamp (300 W) as visible light source. The initial NO concentration used is 500 ppb and the amount of catalyst 0.2 g for all experiments. Before each catalytic experiment, 0.2 g of the sample is dispersed in 10 mL of DI water and evaporated at 80°C and then placed in the dark to achieve adsorption-desorption equilibrium. Finally, the sample is illuminated by Xenon lamp (300 W) for 30 min.

To evaluate the photocatalytic process mechanism for NO degradation, active species trapping experiments are performed. Here, three trapping agents are used representing different active species, namely isopropyl alcohol (IPA) for the hydroxyl radical ( $\bullet\text{OH}$ ), potassium dichromate ( $\text{K}_2\text{Cr}_2\text{O}_7$ ) for the electron ( $e^-$ ) and potassium iodide (KI) for hole ( $h^+$ ). The photocatalytic NO degradation experiments are performed under the same conditions as described previously.

The photocatalytic NO degradation efficiency ( $\eta$ ), the yield of  $\text{NO}_2$  conversion ( $\gamma$ ), the apparent quantum efficiency (AQE) ( $\phi$ ), and DeNOx ( $\alpha_{\text{DeNOx}}$ ) are calculated by the following Eqs.(1-4) [28–30]:

$$\eta = \frac{C_{\text{NO},i} - C_{\text{NO},f}}{C_{\text{NO},i}} \times 100\% \quad (1)$$

$$\gamma = \frac{C_{\text{NO}_2,f} - C_{\text{NO}_2,i}}{C_{\text{NO},i} - C_{\text{NO},f}} \times 100\% \quad (2)$$

$$\phi_{\text{app}} = \frac{N_A \int_0^t (C_{\text{NO},i} - C_{\text{NO},f}) V_t}{\text{Photon Flux} \times \text{Irradiation Area} \times t \times 1000\text{M}} \times 100\% \quad (3)$$

$$\alpha_{\text{DeNOx}} = \eta(1 - 3\gamma) C_{\text{NO},i} \quad (4)$$

where  $C_{\text{NO}}$  is the concentration of NO (ppb),  $C_{\text{NO}_2}$  is the concentration of  $\text{NO}_2$  (ppb),  $i$  is the initial concentration, and  $f$  is the final concentration.  $N_A$  is the Avogadro constant ( $\text{mol}^{-1}$ ),  $V_t$  is the flow rate of NO ( $\text{L min}^{-1}$ ), and  $M$  is the NO molecule weight ( $\text{g mol}^{-1}$ ). The photon flux in the photocatalytic experiment is  $2.72 \cdot 10^{19} \text{ cm}^{-2} \text{ min}^{-1}$ , the irradiation area for the 12 cm diameter petri dish is  $113.1 \text{ cm}^2$ .

In addition, the bandgap energy of materials are calculated by the Tauc and Kubelka Munk equation as describe in Eqs. (5-7) [30]:

$$E = h\nu = \frac{hc}{\lambda} \quad (5)$$

$$(\alpha h\nu)^r = B(h\nu - E_g) \quad (6)$$

$$(F(R)h\nu)^r = B(h\nu - E_g) \quad (7)$$

where E is the photon energy (eV), h is the Planck constant ( $4.132 \times 10^{-15}$  eV.s),  $\nu$  is the photon frequency ( $s^{-1}$ ), c is the photon velocity (nm),  $\lambda$  is the wavelength (nm),  $\alpha$  is the absorption coefficients, B is a constant, and  $E_g$  is the band gap energy (eV), R is reflectance value.

## Results and discussion

### Photocatalytic performance

The photocatalytic NO degradation efficiencies of the materials are depicted in Figure 2a. The photocatalytic NO degradation efficiencies of the materials are gradually increased during the first 5 min of the photocatalytic reaction. And then it stays stable until the end of the photocatalytic reaction. The photocatalytic NO degradation efficiencies are 0.6, 62.8, 16.8, 68.4, 75.4, and 72.1% for the blank sample, g-C<sub>3</sub>N<sub>4</sub>, MgO, 1% MgO@g-C<sub>3</sub>N<sub>4</sub>, 3% MgO@g-C<sub>3</sub>N<sub>4</sub>, 5% MgO@g-C<sub>3</sub>N<sub>4</sub>, respectively. The photocatalytic NO degradation efficiency is increased by combining MgO with g-C<sub>3</sub>N<sub>4</sub>. The results indicate that the MgO@g-C<sub>3</sub>N<sub>4</sub> heterojunction structure has been successfully synthesized with high photocatalytic NO degradation efficiency under visible light by one-step pyrolysis with the ratio of MgO: g-C<sub>3</sub>N<sub>4</sub> is 3:100. On the other hand, the AQE is calculated by [Eqs. 3](#). The AQE (10<sup>-4</sup>%) of the g-C<sub>3</sub>N<sub>4</sub>, MgO, 1% MgO@g-C<sub>3</sub>N<sub>4</sub>, 3% MgO@g-C<sub>3</sub>N<sub>4</sub>, 5% MgO@g-C<sub>3</sub>N<sub>4</sub> are 5.5, 1.4, 5.4, 6.7, and 6.2,

respectively. The AQE results (Figure 2b) show that the photon has more effect on the 3% MgO@g-C<sub>3</sub>N<sub>4</sub> than the others. The heterojunction structure has enhanced the photocatalytic activities of the materials [31]. In addition, the photocatalytic reusability of the 3% MgO@g-C<sub>3</sub>N<sub>4</sub> is investigated by 5 times recycling test in the same experimental conditions (Figure. 2c). The photocatalytic NO degradation efficiency in the recycling test are 75.4, 73.8, 71.1, 69.4, and 68.3% after 5 times respectively. The photocatalytic NO degradation efficiency is decreased 7% after 5 times recycling. The recycling test and the FTIR spectra before and after recycling test (Figure S1) indicate that the 3% MgO@g-C<sub>3</sub>N<sub>4</sub> has high reusability.

On the other hand, the NO conversion to NO<sub>2</sub> and by-products are calculated and shown in Figure 3a. The NO conversion to NO<sub>2</sub> of the g-C<sub>3</sub>N<sub>4</sub>, MgO, 1% MgO@g-C<sub>3</sub>N<sub>4</sub>, 3% MgO@g-C<sub>3</sub>N<sub>4</sub>, 5% MgO@g-C<sub>3</sub>N<sub>4</sub> are 28.2, 7.3, 34.4, 53.5, and 46.3%, respectively. Besides, the NO converts to by-products performance of the g-C<sub>3</sub>N<sub>4</sub>, MgO, 1% MgO@g-C<sub>3</sub>N<sub>4</sub>, 3% MgO@g-C<sub>3</sub>N<sub>4</sub>, 5% MgO@g-C<sub>3</sub>N<sub>4</sub> are 28.2, 7.3, 34.4, 53.5, and 46.3%, respectively. In this study, the by-products are defined as any nitrogen species (N<sub>2</sub>O<sub>5</sub>, N<sub>2</sub>O, NO<sub>3</sub><sup>-</sup>, etc.) that excludes NO<sub>2</sub>, which is very unstable and can be absorbed by the plants [32]. The MgO has the lowest NO<sub>2</sub> and by-products generation due to the lowest photocatalytic NO degradation efficiency (16.8%). Compared with the g-C<sub>3</sub>N<sub>4</sub> and others MgO@g-C<sub>3</sub>N<sub>4</sub>, the 3% MgO@g-C<sub>3</sub>N<sub>4</sub> has the lowest NO<sub>2</sub> (21.9%) and highest by-products (53.5%) generation. In addition, the NO<sub>2</sub> generation of the g-C<sub>3</sub>N<sub>4</sub> and 1% MgO@g-C<sub>3</sub>N<sub>4</sub> are almost equal. This point can be explained due to the amount of MgO being too low (1% only). The 3% MgO@g-C<sub>3</sub>N<sub>4</sub> show the highest photocatalytic NO degradation efficiency with the lowest NO<sub>2</sub> generation, which confirms that the 3% MgO@g-C<sub>3</sub>N<sub>4</sub> can be applied in the future. Besides, the DeNO<sub>x</sub> efficiencies are calculated by [Eqs. 4](#) [33]. The DeNO<sub>x</sub> efficiency

of the g-C<sub>3</sub>N<sub>4</sub>, MgO, 1% MgO@g-C<sub>3</sub>N<sub>4</sub>, 3% MgO@g-C<sub>3</sub>N<sub>4</sub>, 5% MgO@g-C<sub>3</sub>N<sub>4</sub> are -201.6, -58.2, -160.8, 47.4, and -25.8%, respectively.

## The XRD patterns and FTIR spectrum analysis

XRD patterns determine the crystalline phase structure of the synthesized materials in Figure 4a. There are two distinct diffraction peaks at  $2\theta = 13^\circ$  and  $27.4^\circ$ , which are assigned to the (100) and (002) planes of g-C<sub>3</sub>N<sub>4</sub>, respectively [34]. The characteristic diffraction peaks of MgO are detected to be  $36.9^\circ$ ,  $42.9^\circ$ ,  $62.5^\circ$ ,  $74.8^\circ$ , and  $78.7^\circ$ , which are attributed to the (111), (200), (220), (311), and (222) planes, respectively [35, 36]. With different MgO mass ratios, the MgO@g-C<sub>3</sub>N<sub>4</sub> composites still retain the peak characteristics of g-C<sub>3</sub>N<sub>4</sub>. No impurities are detected in the XRD samples of MgO@g-C<sub>3</sub>N<sub>4</sub>, indicating that the prepared synthetic material possessed high purity. The characteristic peaks of MgO that are not detected in all synthesized MgO@g-C<sub>3</sub>N<sub>4</sub> samples are attributed to the low amount of MgO in the composite. This point agrees with previous studies, which indicated that the characteristic peak of MgO is detected as MgO is added with an amount higher than 5% [22, 37].

Figure 4b illustrates the FTIR spectrum of g-C<sub>3</sub>N<sub>4</sub>, MgO, and MgO@g-C<sub>3</sub>N<sub>4</sub>, respectively. For pure g-C<sub>3</sub>N<sub>4</sub>, the broad peak in the range  $3000 - 3600 \text{ cm}^{-1}$  is attributed to the stretching vibrations of N-H and O-H bonds, indicating the existence of amino groups and adsorbed water molecules in the material [21, 38]. The characteristic peaks at  $1240$ ,  $1320$ ,  $1407$ , and  $1465 \text{ cm}^{-1}$  are associated with the stretching vibration of the aromatic C-N bond, and typical peaks at  $1562$  and  $1642 \text{ cm}^{-1}$  characterize the presence of C=O bond [39, 40]. In addition, the characteristic peak at  $810 \text{ cm}^{-1}$  matches up with the typical breathing mode of the triazine unit. After adding MgO, the distinct peaks of all MgO@g-C<sub>3</sub>N<sub>4</sub> composites showed similarity to

that of pure g-C<sub>3</sub>N<sub>4</sub>, indicating that the crystal structure of g-C<sub>3</sub>N<sub>4</sub> remains unchanged. This result is in good agreement with the XRD patterns. In addition, the small peak at 419 cm<sup>-1</sup> proves the presence of MgO in the MgO@g-C<sub>3</sub>N<sub>4</sub> composites [41].

The morphology of g-C<sub>3</sub>N<sub>4</sub>, MgO, and 3%MgO@g-C<sub>3</sub>N<sub>4</sub> are determined through SEM and TEM analysis. The typical bulk structure of the g-C<sub>3</sub>N<sub>4</sub> is observed in Fig. 5(e, f). Besides, the difference between the morphology of MgO and g-C<sub>3</sub>N<sub>4</sub> is difficult to observe by SEM (Figure 5c, d). Figure 5a, and Figure 5b show that the morphology 3%MgO@g-C<sub>3</sub>N<sub>4</sub> is similar to pure g-C<sub>3</sub>N<sub>4</sub>. The obtained results indicate that the morphology of 3% MgO@g-C<sub>3</sub>N<sub>4</sub> is identical to that of g-C<sub>3</sub>N<sub>4</sub> because the adding amount of MgO is too low, as determined by EDS mapping. The EDS mapping images of the 3% MgO@g-C<sub>3</sub>N<sub>4</sub> are shown in Figure 6 and Figure S2. The wt% of C, N, Mg, and O is 37%, 52%, 9%, and 2%, respectively. As shown in Figure 6, the wt% of Mg and O are lowest, indicating that the amount of MgO into the composites is too low. The shape of the g-C<sub>3</sub>N<sub>4</sub> is easy to observe in Figure 7c, d. However, the shape of MgO are complicated to determine by TEM and HR-TEM (Figure 7a, b). These results emphasized the presence of MgO in the compound, which is identified and documented by XRD and SEM-EDS mapping.

## **The element states analysis**

The XPS and HR-XPS are invested in determining the element states of the materials. The XPS surveys of the g-C<sub>3</sub>N<sub>4</sub> MgO and 3% MgO@g-C<sub>3</sub>N<sub>4</sub> are shown in Figure 8a. The peaks at 87 and 530 eV are assigned to the Mg 2s and O 1s of the MgO, respectively. The peaks at 287 and 397 eV assigned to the C 1s and N 1s of the g-C<sub>3</sub>N<sub>4</sub>, respectively [12, 42, 43]. In the MgO, the peaks of Mg 2p, Mg KLL, O loss, and O KLL are observed at 46, 304, 555, and 978 eV, respectively [44, 45]. The HR-XPS

of the C 1s are shown in Figure 8b, the peaks at 283 eV assigned to the C–C coordination in the MgO, and the peaks at 287 eV assigned to the N–C=N bonds of the g-C<sub>3</sub>N<sub>4</sub>, and these bonds only appear on the samples g-C<sub>3</sub>N<sub>4</sub>, and 3% MgO@g-C<sub>3</sub>N<sub>4</sub>. However, the C1s peak of MgO and g-C<sub>3</sub>N<sub>4</sub> occurs together in the 3% MgO@g-C<sub>3</sub>N<sub>4</sub>. These results confirm that the C 1s of the material doesn't change during the pyrolysis method. The HR-XPS of N 1s of the materials is shown in Figure 8c, the peaks at 397 and 399 eV correspond to the C–N=C bonds and N–(C)<sub>3</sub> structure of the g-C<sub>3</sub>N<sub>4</sub> [46]. Figure 8d shows the peaks of Mg–O bonds of the MgO at 398 eV [47]. The Mg 2s peaks of the MgO are demonstrated in Figure 8e, f. The peak at 87 eV (Figure 8e), and 87 eV (Figure 8f) confirmed the metallic state of Mg [48]. The peaks of O 1s and Mg 2s of the 3% MgO@g-C<sub>3</sub>N<sub>4</sub> are too weak.

## **The optical properties of the materials**

The DRS spectra are invested in understanding the optical absorption characteristics of the materials (Figure 9). The g-C<sub>3</sub>N<sub>4</sub> has a significant light absorption capacity at the peak around 440 nm corresponding to the direct and indirect bandgap of 2.83 and 2.7 eV, respectively (Figure 9b, d). Meanwhile, MgO materials with wide bandgap properties show absorption below 400 nm in both Kubelka-Munk and Tauc plots (Figure 9a, c). After adding MgO into g-C<sub>3</sub>N<sub>4</sub>, the MgO@g-C<sub>3</sub>N<sub>4</sub> materials slightly shift to the visible light region. The optical direct and indirect bandgap energy is slightly reduced, corresponding to the increase in MgO proportion. The bandgap reduction can be attributed to Mg–N bonds in the MgO@g-C<sub>3</sub>N<sub>4</sub> materials that promote charge transport, thus increasing the photocatalytic efficiency [22, 37]. Generally, this result indicates the existence of MgO in the MgO@g-C<sub>3</sub>N<sub>4</sub> material, which is difficult to demonstrate by the previous analysis.

## Photocatalytic mechanism

Trapping experiments are carried out to evaluate the involvement of electrons, holes, and reactive oxygen species (ROSs), including KI ( $h^+$ ),  $K_2Cr_2O_7$  ( $e^-$ ), and IPA ( $\bullet OH$ ). Figure 10a shows the reduction in process efficiency under scavengers. In detail, the photocatalytic NO degradation efficiency decreases significantly from 75.4% to 36.4% in the existence of KI. In addition, the existence of  $K_2Cr_2O_7$  as a representative for  $e^-$  also contributes to NO decomposition, reducing 1.3 times compared to the original efficiency. Finally, the weak participation of  $\bullet OH$  radicals in the NO degradation is clearly described, with a reduction in efficiency of only about 1%. Hence, KI and  $K_2Cr_2O_7$  are the main factors that significantly influence the NO photocatalytic degradation performance.

Besides, ESR is invested in determining the reaction mechanism of the material accurately. Figure 10b shows that under Visible light and DMPO– $H_2O$  and DMPO–OH, this material both generates  $\bullet OH$  and  $\bullet O_2$  radicals. In contrast, only  $\bullet OH$  radicals are generated under dark conditions, but the intensity is fragile. Hence, the generation of  $\bullet O_2$  radicals contributes significantly to the photocatalytic NO degradation efficiency.

The photocatalysis mechanism of  $MgO@g-C_3N_4$  is proposed through the analyses mentioned above, as illustrated in Figure 11. Under visible light, only  $g-C_3N_4$  is excited to produce an  $e^-h^+$  pairs. Due to the negative valence band (VB) potential of  $g-C_3N_4$  (+1.75 eV) compared to  $H_2O/\bullet OH$  potential (+2.40 eV) and  $\bullet OH/OH^-$  potential (+1.99 eV), the  $h^+$  cannot react with  $H_2O$  to produce an  $\bullet OH$  radicals for the reduction reaction [49]. Simultaneously, at the CB of  $g-C_3N_4$ , the  $e^-$  is excited and reacts with  $H_2O$  to produce  $\bullet O_2^-$  radicals. In addition, this  $e^-$  also migrates across the CB of MgO, creating

an excess  $e^-$  in MgO and avoiding recombination at g-C<sub>3</sub>N<sub>4</sub>. This  $e^-$  reacts with H<sub>2</sub>O to produce  $\bullet O_2^-$  radicals. This  $\bullet O_2^-$  radicals decompose NO to produce NO<sub>2</sub> and by-products. In addition, the  $h^+$  at the VB of MgO are thought to react with H<sub>2</sub>O to give  $\bullet OH$ . Also, this  $\bullet OH$  decomposes NO, creating NO<sub>2</sub> and by-products. This reason is supported and explained by ESR and trapping tests.

## Conclusion

In conclusion, the MgO@g-C<sub>3</sub>N<sub>4</sub> heterojunctions were effectively synthesized by one-step pyrolysis of the commercial MgO and Urea. The photocatalytic efficiencies of the synthesized materials were increased dramatically by mixing MgO and g-C<sub>3</sub>N<sub>4</sub>. The results indicated that 3%MgO@g-C<sub>3</sub>N<sub>4</sub> possessed the highest NO photodegradation efficiency, reaching 75.4%. In addition, the photocatalytic NO degradation efficiency of the composite was decreased when the amount of MgO exceeded 3%. The enhanced appearance quantum efficiency ( $6.7 \times 10^{-4}\%$ ), as well as long time-life recombination of  $e^-$  based on the heterojunction structure, was formed by combining MgO and g-C<sub>3</sub>N<sub>4</sub> attributed to being the reason leading to the highest NO photodegradation efficiency of 3%MgO@g-C<sub>3</sub>N<sub>4</sub> sample. Moreover, the NO conversion to NO<sub>2</sub> and by-products of the 3% MgO@g-C<sub>3</sub>N<sub>4</sub> were lowest (21.9%) and highest (53.5%), respectively. On the other hand, the 3% MgO@g-C<sub>3</sub>N<sub>4</sub> showed high reusability after five times recycling test, the photocatalytic NO degradation efficiency of the 3% MgO@g-C<sub>3</sub>N<sub>4</sub> was decreased 7.1%. The photocatalytic activity results indicated that the 3% MgO@g-C<sub>3</sub>N<sub>4</sub> could be applied in the future as an excellent photocatalyst with high degradation efficiency and low toxic generation. The characterization of the materials was studied by FTIR, XRD, XPS, SEM, TEM, EDS, DRS, and ESR. The apparent of MgO into the composites were difficult to observe by

XRD, SEM, and TEM. So, the FTIR, XPS, and EDS mapping were carried out to confirm the appearance of MgO in the composites. Although the MgO was difficult to determine into the composites, the addition of MgO affected the optical properties of the composites, which increased the photocatalytic performance of the composites. The DRS result displayed that the bandgap of the composites decreased by adding more MgO. Based on the high photocatalytic NO degradation efficiency under visible light and high reusability, the MgO@g-C<sub>3</sub>N<sub>4</sub> was promised to scalable fabrication. Finally, this study provided a new understanding of the photocatalytic performance of MgO@g-C<sub>3</sub>N<sub>4</sub> with the suitable amount of MgO added.

## **Supporting Information**

Supporting information text

Supporting Information File 1:

File Name: Supporting Information

File Format: Word

Title: Additional figures

## **Acknowledgement**

This work was supported by Department of Civil Engineering Chung Yuan Christian University, Taoyuan City, 32023, Taiwan; Department of Environmental Engineering, Chung Yuan Christian University, Taoyuan City, 32023, Taiwan; Center for Environmental Risk Management, Chung Yuan Christian University, No.200, Taoyuan City, 32023, Taiwan; Faculty of Environment and Natural Resources, Ho Chi Minh City University of Technology (HCMUT), VNU-HCM, Vietnam.

## Funding

This research was financially supported by the Chung Yuan Christian University, Taiwan (Project No: [109609432](#))

## References

1. Van Viet, P., Hoang The Vinh, T., Thi Ngoc Dung, N., Minh Thi, C.: Facile ball-milling synthesis of TiO<sub>2</sub> modified ZnO for efficient photocatalytic removal of atmospheric nitric oxide gas under solar light irradiation. *Chem. Phys. Lett.* (2021) 775, 138642. <https://doi.org/10.1016/j.cplett.2021.138642>
2. Zhou, S., Young, C.J., VandenBoer, T.C., Kahan, T.F.: Role of location, season, occupant activity, and chemistry in indoor ozone and nitrogen oxide mixing ratios. *Environ. Sci. Process. Impacts.* (2019) 21, 1374–1383. <https://doi.org/10.1039/C9EM00129H>
3. Pham, M.-T., Hussain, A., Bui, D.-P., Nguyen, T.-M.T., You, S.-J., Wang, Y.-F.: Surface plasmon resonance enhanced photocatalysis of Ag nanoparticles-decorated Bi<sub>2</sub>S<sub>3</sub> nanorods for NO degradation. *Environ. Technol. Innov.* (2021) 23, 101755. <https://doi.org/10.1016/j.eti.2021.101755>
4. Nguyen, V., Nguyen, B., Huang, C., Le, T., Thang, Q., Shokouhimehr, M., Xia, C.: Photocatalytic NO<sub>x</sub> abatement : Recent advances and emerging trends in the development of photocatalysts. *J. Clean. Prod.* (2020) 270, 121912. <https://doi.org/10.1016/j.jclepro.2020.121912>
5. Asghar, U., Rafiq, S., Anwar, A., Iqbal, T., Ahmed, A., Jamil, F., Khurram, M.S., Akbar, M.M., Farooq, A., Shah, N.S., Park, Y.K.: Review on the progress in emission

- control technologies for the abatement of CO<sub>2</sub>, SO<sub>x</sub> and NO<sub>x</sub> from fuel combustion. *J. Environ. Chem. Eng.* (2021) 9, 106064. <https://doi.org/10.1016/j.jece.2021.106064>
6. Qie, F., Zhu, J., Rong, J., Zong, B.: Biological removal of nitrogen oxides by microalgae, a promising strategy from nitrogen oxides to protein production. *Bioresour. Technol.* (2019) 292, 122037. <https://doi.org/10.1016/j.biortech.2019.122037>
  7. Wang, S., Xu, S., Gao, S., Xiao, P., Jiang, M., Zhao, H.: Simultaneous removal NO<sub>x</sub> from flue gas of - SO<sub>2</sub> and - by low - temperature adsorption over activated carbon. *Sci. Rep.* (2021) 11, 11003. <https://doi.org/10.1038/s41598-021-90532-9>
  8. Chen, R., Zhang, T., Guo, Y., Wang, J., Wei, J., Yu, Q.: Recent advances in simultaneous removal of SO<sub>2</sub> and NO<sub>x</sub> from exhaust gases : Removal process , mechanism and kinetics. *Chem. Eng. J.* (2021) 420, 127588. <https://doi.org/10.1016/j.cej.2020.127588>
  9. Talebizadeh, P., Babaie, M., Brown, R., Rahimzadeh, H., Ristovski, Z., Arai, M.: The role of non-thermal plasma technique in NO<sub>x</sub> treatment: A review. *Renew. Sustain. Energy Rev.* (2014) 40, 886–901. <https://doi.org/10.1016/j.rser.2014.07.194>
  10. He, F., Jeon, W., Choi, W.: Photocatalytic air purification mimicking the self-cleaning process of the atmosphere. *Nat. Commun.* (2021) 12, 2528. <https://doi.org/10.1038/s41467-021-22839-0>
  11. Wang, S., Li, C., Wang, T., Zhang, P., Li, A., Gong, J.: Controllable synthesis of nanotube-type graphitic C<sub>3</sub>N<sub>4</sub> and their visible-light photocatalytic and fluorescent properties. *J. Mater. Chem. A.* (2014) 2, 2885–2890. <https://doi.org/10.1039/C3TA14576J>

12. Papailias, I., Todorova, N., Giannakopoulou, T., Karapati, S., Boukos, N., Dimotikali, D., Trapalis, C.: Enhanced NO<sub>2</sub> abatement by alkaline-earth modified g-C<sub>3</sub>N<sub>4</sub> nanocomposites for efficient air purification. *Appl. Surf. Sci.* (2018) 430, 225–233. <https://doi.org/10.1016/j.apsusc.2017.08.084>
13. Pham, V.V., Mai, D.-Q., Bui, D.-P., Van Man, T., Zhu, B., Zhang, L., Sangkaworn, J., Tantirungrotechai, J., Reutrakul, V., Cao, T.M.: Emerging 2D/0D g-C<sub>3</sub>N<sub>4</sub>/SnO<sub>2</sub> S-scheme photocatalyst: New generation architectural structure of heterojunctions toward visible-light-driven NO degradation. *Environ. Pollut.* (2021) 286, 117510. <https://doi.org/10.1016/j.envpol.2021.117510>
14. Hoang The Vinh, T., Minh Thi, C., Van Viet, P.: Enhancing photocatalysis of NO gas degradation over g-C<sub>3</sub>N<sub>4</sub> modified  $\alpha$ -Bi<sub>2</sub>O<sub>3</sub> microrods composites under visible light. *Mater. Lett.* (2020) 281, 128637. <https://doi.org/10.1016/j.matlet.2020.128637>
15. Zhao, G.-Q., Zou, J., Hu, J., Long, X., Jiao, F.-P.: A critical review on graphitic carbon nitride (g-C<sub>3</sub>N<sub>4</sub>)-based composites for environmental remediation. *Sep. Purif. Technol.* (2021) 279, 119769. <https://doi.org/10.1016/j.seppur.2021.119769>
16. Van, K.N., Huu, H.T., Nguyen Thi, V.N., Le Thi, T.L., Truong, D.H., Truong, T.T., Dao, N.N., Vo, V., Tran, D.L., Vasseghian, Y.: Facile construction of S-scheme SnO<sub>2</sub>/g-C<sub>3</sub>N<sub>4</sub> photocatalyst for improved photoactivity. *Chemosphere.* (2022) 289, 133120. <https://doi.org/10.1016/j.chemosphere.2021.133120>
17. Mousavi, M., Habibi-Yangjeh, A., Pournan, S.R.: Review on magnetically separable graphitic carbon nitride-based nanocomposites as promising visible-light-driven photocatalysts. *J. Mater. Sci. Mater. Electron.* (2018) 29, 1719–1747. <https://doi.org/10.1007/s10854-017-8166-x>
18. Madona, J., Sridevi, C.: Surfactant assisted hydrothermal synthesis of MgO/g-C<sub>3</sub>N<sub>4</sub>

- heterojunction nanocomposite for enhanced solar photocatalysis and antimicrobial activities. *Inorg. Chem. Commun.* (2022) 138, 109265.  
<https://doi.org/10.1016/j.inoche.2022.109265>
19. Huang, Z., Zhao, X., Xia, H., Lu, F., Hu, L., Chu, P.K.: Insights into enhancement of photocatalytic properties of g-C<sub>3</sub>N<sub>4</sub> by local electric field induced by polarization of MgO(111). *J. Environ. Chem. Eng.* (2021) 9, 105922.  
<https://doi.org/10.1016/j.jece.2021.105922>
  20. Sharmin, F., Chandra Roy, D., Basith, M.A.: Photocatalytic water splitting ability of Fe/MgO-rGO nanocomposites towards hydrogen evolution. *Int. J. Hydrogen Energy.* (2021) 46, 38232–38246. <https://doi.org/10.1016/j.ijhydene.2021.09.072>
  21. An, W., Tian, L., Hu, J., Liu, L., Cui, W., Liang, Y.: Efficient degradation of organic pollutants by catalytic ozonation and photocatalysis synergy system using double-functional MgO/g-C<sub>3</sub>N<sub>4</sub> catalyst. *Appl. Surf. Sci.* (2020) 534, 147518.  
<https://doi.org/10.1016/j.apsusc.2020.147518>
  22. Li, N., Huang, M., Zhou, J., Liu, M., Jing, D.: MgO and Au nanoparticle Co-modified g-C<sub>3</sub>N<sub>4</sub> photocatalysts for enhanced photoreduction of CO<sub>2</sub> with H<sub>2</sub>O. *Chinese J. Catal.* (2021) 42, 781–794. [https://doi.org/10.1016/S1872-2067\(20\)63690-7](https://doi.org/10.1016/S1872-2067(20)63690-7)
  23. Ge, L., Peng, Z., Wang, W., Tan, F., Wang, X., Su, B., Qiao, X., Wong, P.K.: g-C<sub>3</sub>N<sub>4</sub>/MgO nanosheets: light-independent, metal-poisoning-free catalysts for the activation of hydrogen peroxide to degrade organics. *J. Mater. Chem. A.* (2018) 6, 16421–16429. <https://doi.org/10.1039/C8TA05488F>
  24. Shelemanov, A.A., Evstropiev, S.K., Karavaeva, A. V, Nikonorov, N. V, Vasilyev, V.N., Podruhin, Y.F., Kiselev, V.M.: Enhanced singlet oxygen photogeneration by bactericidal ZnO–MgO–Ag nanocomposites. *Mater. Chem. Phys.* (2022) 276, 125204.

<https://doi.org/10.1016/j.matchemphys.2021.125204>

25. Panchal, P., Paul, D.R., Sharma, A., Hooda, D., Yadav, R., Meena, P., Nehra, S.P.: Phytoextract mediated ZnO/MgO nanocomposites for photocatalytic and antibacterial activities. *J. Photochem. Photobiol. A Chem.* (2019) 385, 112049.  
<https://doi.org/10.1016/j.jphotochem.2019.112049>
26. Bekena, F., Kuo, D.-H.: 10 nm sized visible light TiO<sub>2</sub> photocatalyst in the presence of MgO for degradation of methylene blue. *Mater. Sci. Semicond. Process.* (2020) 116, 105152. <https://doi.org/10.1016/j.mssp.2020.105152>
27. Chen, J., Xiong, J., Song, Y., Yu, Y., Wu, L.: Synthesis of nitrosobenzene via photocatalytic oxidation of aniline over MgO/TiO<sub>2</sub> under visible light irradiation. *Appl. Surf. Sci.* (2018) 440, 1269–1276. <https://doi.org/10.1016/j.apsusc.2018.01.228>
28. Guerrand, H., Pucheault, M., Vaultier, M.: Ionic liquids. *Green Proc. Eng.* (2015)
29. Ohtani, B.: Chapter 10 - Photocatalysis by inorganic solid materials: Revisiting its definition, concepts, and experimental procedures. In: Eldik, R. van and Stochel, G.B.T.-A. in I.C. (eds.) *Inorganic Photochemistry*. pp. 395–430. Academic Press (2011)
30. Bui, D.-P., Pham, M.-T., Tran, H.-H., Nguyen, T.-D., Cao, T.M., Pham, V. Van: Revisiting the Key Optical and Electrical Characteristics in Reporting the Photocatalysis of Semiconductors. *ACS Omega.* (2021) 6, 27379–27386.  
<https://doi.org/10.1021/acsomega.1c04215>
31. Pham, M.-T., Luu, H.Q., Nguyen, T.M.T., Tran, H.H., You, S.J., Wang, Y.F.: Rapid and Scalable Fabrication of TiO<sub>2</sub>@g-C<sub>3</sub>N<sub>4</sub> Heterojunction for Highly Efficient Photocatalytic NO Removal under Visible Light. *Aerosol Air Qual. Res.* (2021) 21, 1–

15. <https://doi.org/10.4209/AAQR.210276>
32. Roy, S., Madras, G.: Photocatalytic NO<sub>x</sub> Abatement: A Short Review, <http://www.eurekaselect.com/article/67866>, (2015)
33. Pham, M.-T., Tran, H.-H., Nguyen, T.-M.T., Bui, D.-P., Huang, Y., Cao, J., You, S.-J., Van Viet, P., Nam, V.H., Wang, Y.-F.: Revealing DeNO<sub>x</sub> and DeVOC Reactions via the Study of the Surface and Bandstructure of ZnSn(OH)<sub>6</sub> Photocatalysts. *Acta Mater.* (2021) 215, 117068. <https://doi.org/10.1016/j.actamat.2021.117068>
34. Kumar, A., Singh, S., Khanuja, M.: A comparative photocatalytic study of pure and acid-etched template free graphitic C<sub>3</sub>N<sub>4</sub> on different dyes: An investigation on the influence of surface modifications. *Mater. Chem. Phys.* (2020) 243, 122402. <https://doi.org/10.1016/j.matchemphys.2019.122402>
35. Xu, L., Gao, S., Chen, M., Wu, Y., Shinozaki, K.: Improvement in microstructure and thermo-mechanical properties of MgO-based dry vibratable material by addition of Fe. *Mater. Chem. Phys.* (2020) 253, 123368. <https://doi.org/10.1016/j.matchemphys.2020.123368>
36. Mohammed, W.M., Yanilkin, I. V, Gumarov, A.I., Kiiamov, A.G., Yusupov, R. V, Tagirov, L.R.: Epitaxial growth and superconducting properties of thin-film PdFe/VN and VN/PdFe bilayers on MgO(001) substrates. *Beilstein J. Nanotechnol.* (2020) 11, 807–813
37. Mao, N., Jiang, J.-X.: MgO/g-C<sub>3</sub>N<sub>4</sub> nanocomposites as efficient water splitting photocatalysts under visible light irradiation. *Appl. Surf. Sci.* (2019) 476, 144–150. <https://doi.org/10.1016/j.apsusc.2019.01.049>
38. Yuan, Y., Zhang, L., Xing, J., Utama, M.I.B., Lu, X., Du, K., Li, Y., Hu, X., Wang, S.,

- Genç, A., Dunin-Borkowski, R., Arbiol, J., Xiong, Q.: High-yield synthesis and optical properties of g-C<sub>3</sub>N<sub>4</sub>. *Nanoscale*. (2015) 7, 12343–12350.  
<https://doi.org/10.1039/C5NR02905H>
39. Chen, Z., Sun, P., Fan, B., Liu, Q., Zhang, Z., Fang, X.: Textural and electronic structure engineering of carbon nitride via doping with  $\pi$ -deficient aromatic pyridine ring for improving photocatalytic activity. *Appl. Catal. B Environ.* (2015) 170–171, 10–16. <https://doi.org/10.1016/j.apcatb.2015.01.024>
40. Bojdys, M.J., Müller, J.-O., Antonietti, M., Thomas, A.: Ionothermal Synthesis of Crystalline, Condensed, Graphitic Carbon Nitride. *Chem. – A Eur. J.* (2008) 14, 8177–8182. <https://doi.org/10.1002/chem.200800190>
41. Dobrucka, R.: Synthesis of MgO Nanoparticles Using *Artemisia abrotanum* Herba Extract and Their Antioxidant and Photocatalytic Properties. *Iran. J. Sci. Technol. Trans. A Sci.* (2018) 42, 547–555. <https://doi.org/10.1007/s40995-016-0076-x>
42. Li, D., Xiao, Y., Pu, M., Zan, J., Zuo, S., Xu, H., Xia, D.: A metal-free protonated g-C<sub>3</sub>N<sub>4</sub> as an effective sodium percarbonate activator at ambient pH conditions: Efficiency, stability and mechanism. *Mater. Chem. Phys.* (2019) 231, 225–232. <https://doi.org/10.1016/j.matchemphys.2019.04.016>
43. Tan, L., Xu, J., Zhang, X., Hang, Z., Jia, Y., Wang, S.: Synthesis of g-C<sub>3</sub>N<sub>4</sub>/CeO<sub>2</sub> nanocomposites with improved catalytic activity on the thermal decomposition of ammonium perchlorate. *Appl. Surf. Sci.* (2015) 356, 447–453. <https://doi.org/10.1016/j.apsusc.2015.08.078>
44. Cimino, A.: X-ray photoelectron spectroscopy (XPS) analysis of oxide solid solutions. *Mater. Chem. Phys.* (1985) 13, 221–241. [https://doi.org/https://doi.org/10.1016/0254-0584\(85\)90057-4](https://doi.org/https://doi.org/10.1016/0254-0584(85)90057-4)

45. Peng, Q., Dai, Y., Liu, K., Luo, X., He, D., Tang, X., Huang, G.: A novel carbon nanotube–magnesium oxide composite with excellent recyclability to efficiently activate peroxymonosulfate for Rhodamine B degradation. *J. Mater. Sci.* (2020) 55, 11267–11283. <https://doi.org/10.1007/s10853-020-04822-0>
46. Wang, P., Guan, Z., Li, Q., Yang, J.: Efficient visible-light-driven photocatalytic hydrogen production from water by using Eosin Y-sensitized novel g-C<sub>3</sub>N<sub>4</sub>/Pt/GO composites. *J. Mater. Sci.* (2018) 53, 774–786. <https://doi.org/10.1007/s10853-017-1540-5>
47. Vesali-Kermani, E., Habibi-Yangjeh, A., Ghosh, S.: Visible-light-induced nitrogen photofixation ability of g-C<sub>3</sub>N<sub>4</sub> nanosheets decorated with MgO nanoparticles. *J. Ind. Eng. Chem.* (2020) 84, 185–195. <https://doi.org/10.1016/j.jiec.2019.12.033>
48. Gu, W., Lee, J.T., Nitta, N., Yushin, G.: Electrodeposition of Nanostructured Magnesium Coatings. *Nanomater. Nanotechnol.* (2014) 4, 30. <https://doi.org/10.5772/59931>
49. Van Pham, V., Tran, H.-H., Truong, T.K., Cao, T.M.: Tin dioxide nanomaterial-based photocatalysts for nitrogen oxide oxidation: a review. *Beilstein J. Nanotechnol.* (2022) 13, 96–113

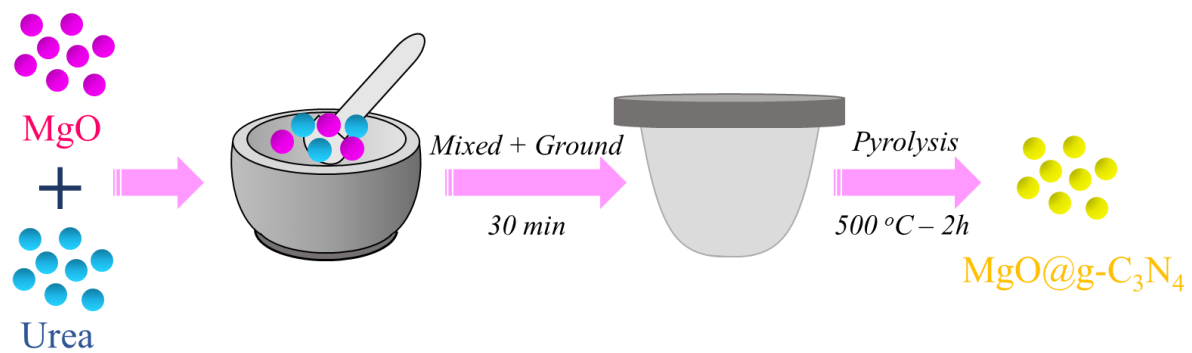


**Figure 1:** Schematic diagram of pyrolysis synthesis process for MgO@g-C<sub>3</sub>N<sub>4</sub> composite.

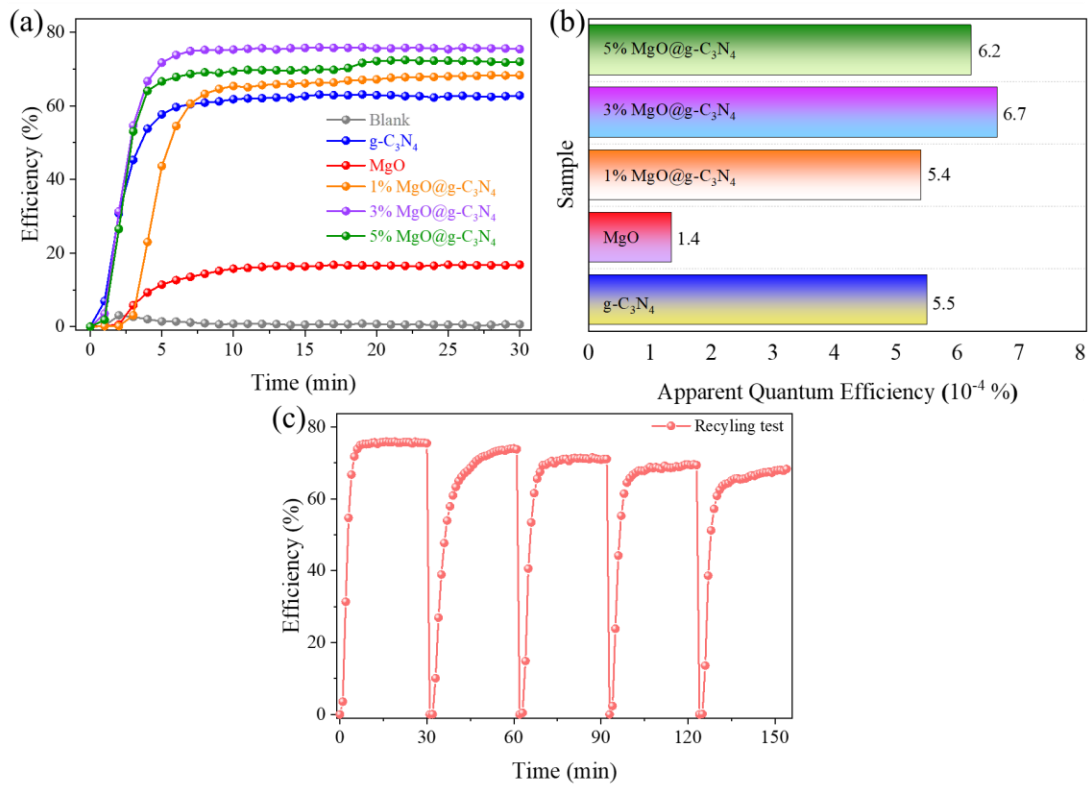


**Figure 2:** Photocatalytic NO degradation efficiency (a), Apparent quantum efficiency of the materials (b), and Photocatalytic recycling test of the 3% MgO@g-C<sub>3</sub>N<sub>4</sub> (c).

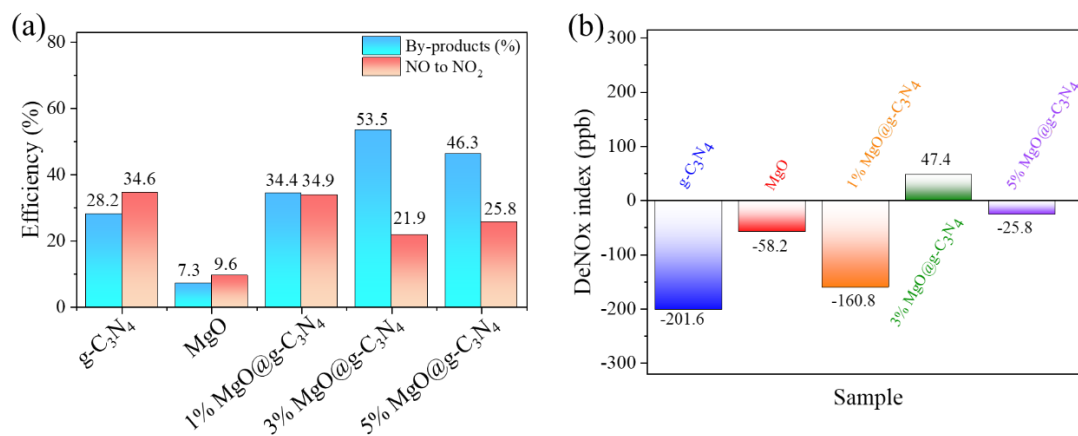


**Figure 3:** NO conversion (a), and DeNOx index of the materials (b).

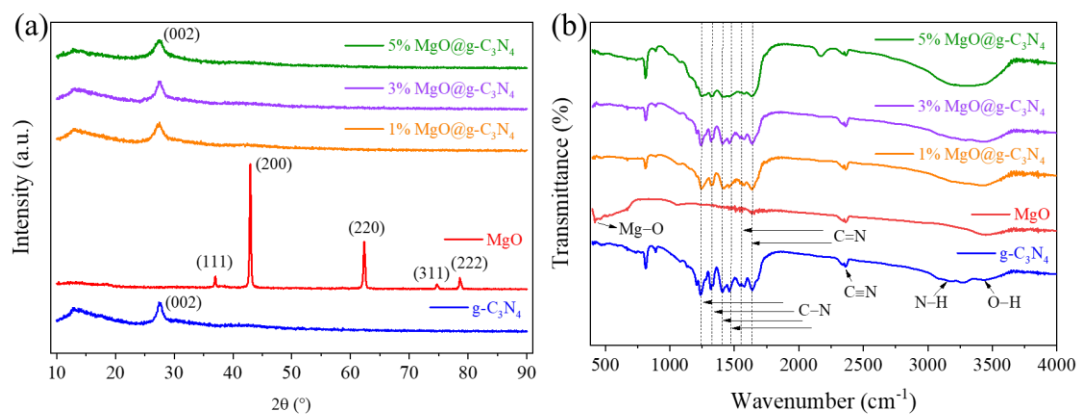


**Figure 4:** The XRD patterns (a), and FTIR spectra of the materials (b).

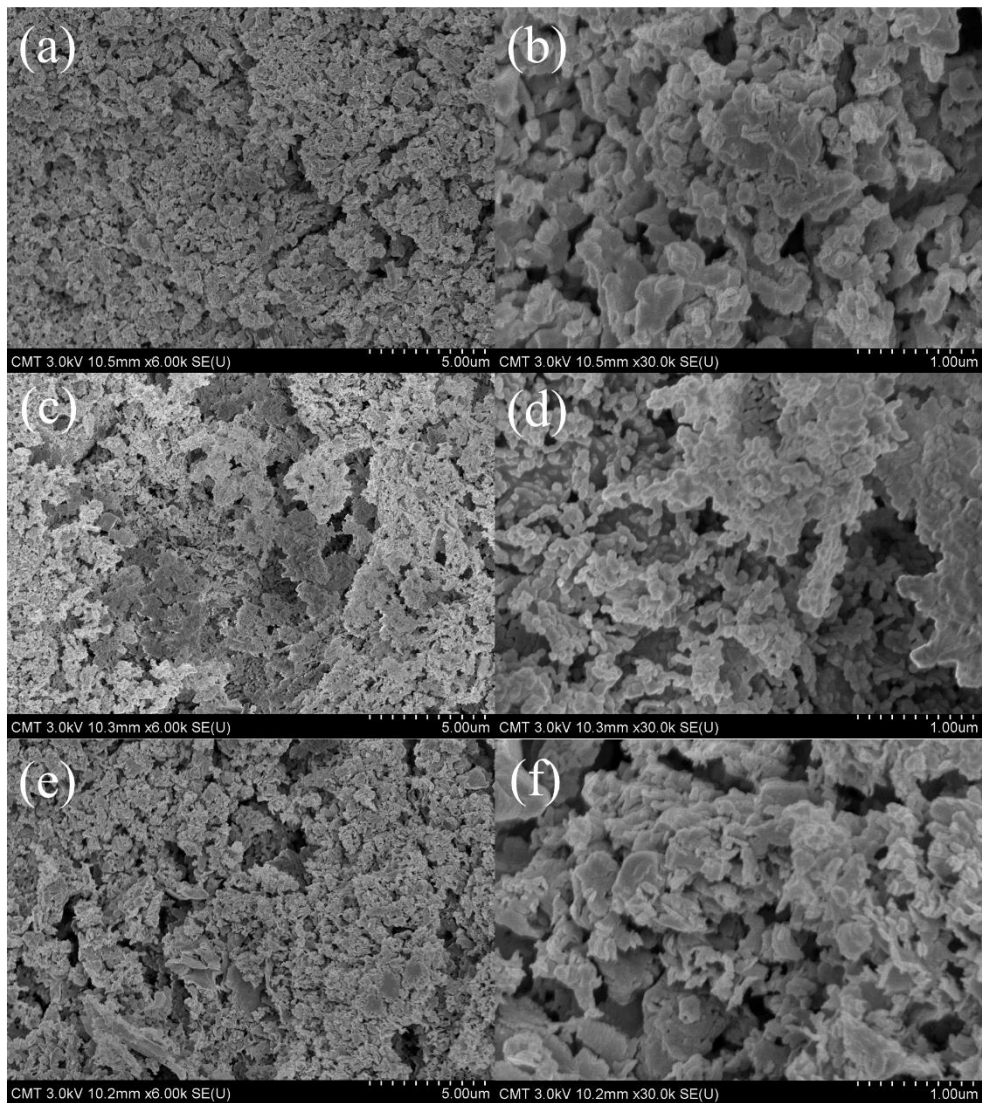


**Figure 5:** SEM images of 3%MgO@g-C<sub>3</sub>N<sub>4</sub> (a, b), MgO (c, d), and g-C<sub>3</sub>N<sub>4</sub> (d, f).

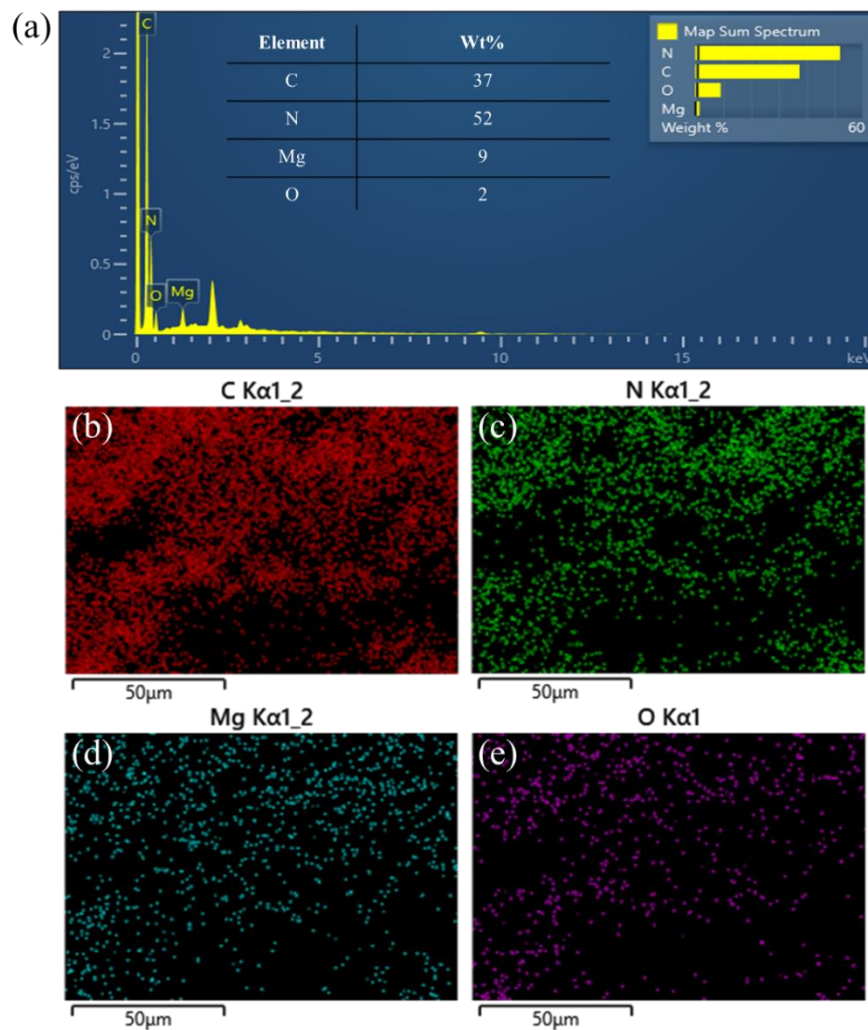


**Figure 6:** The SEM-EDS (a), and EDS-mapping of the 3% MgO@g-C<sub>3</sub>N<sub>4</sub> (b-e).

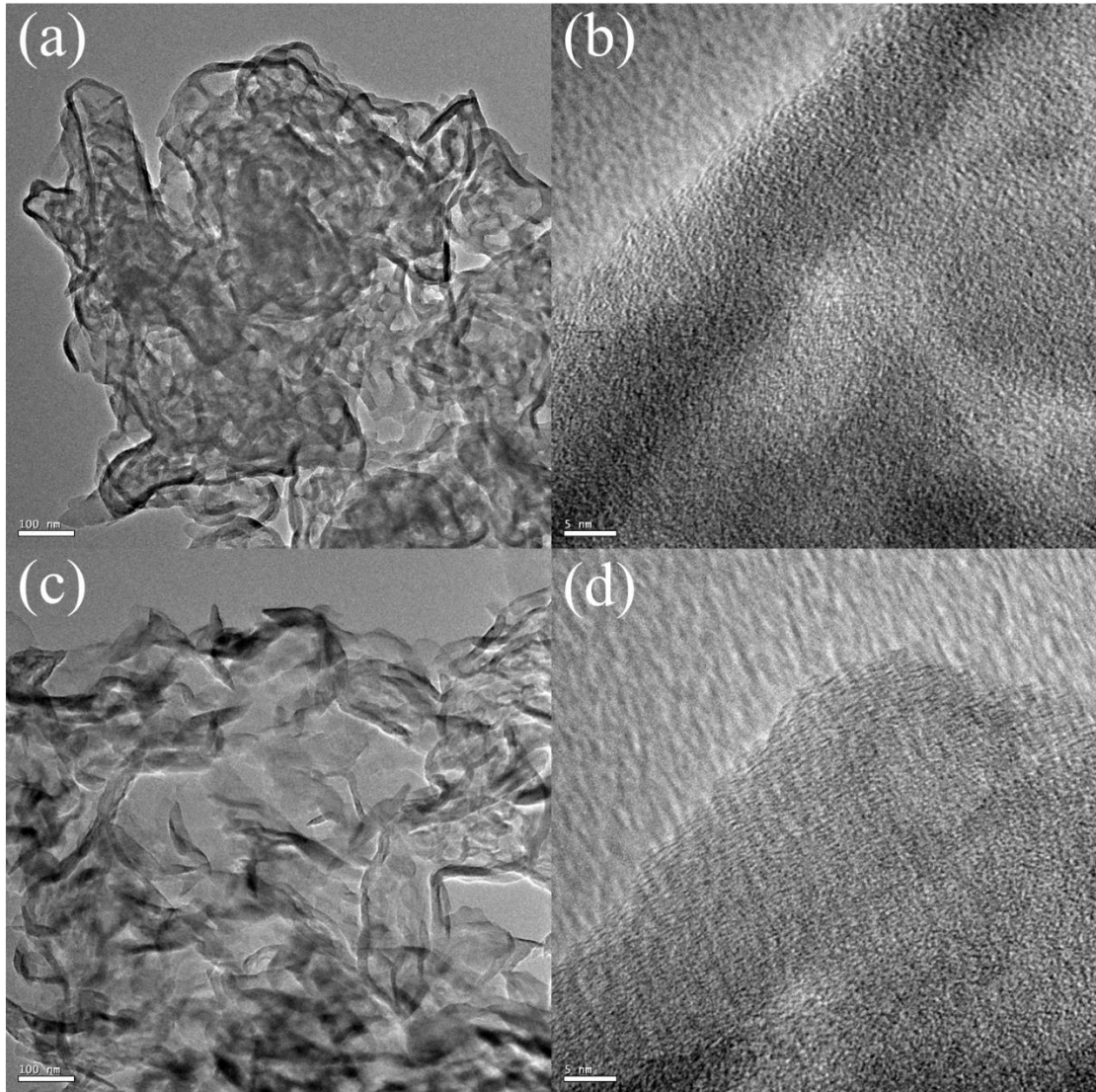


**Figure 7:** The TEM and HR-TEM of the MgO@g-C<sub>3</sub>N<sub>4</sub> (a, b), and g-C<sub>3</sub>N<sub>4</sub> (c, d).

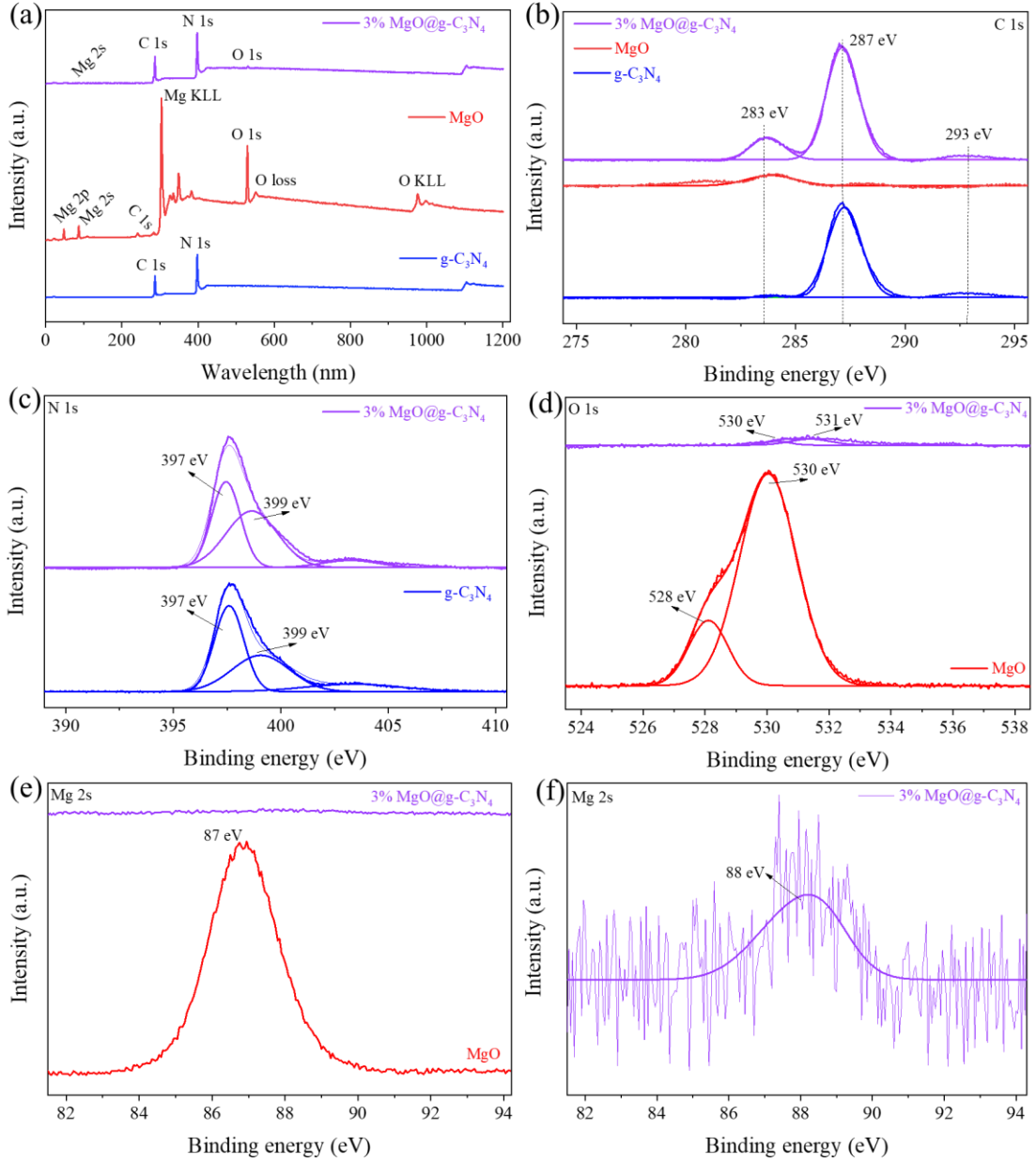


**Figure 8:** The XPS survey (a), HR-XPS C 1s (b), N 1s (c), O 1s (d), C 1s (c), and Mg 2s (e, f) of the materials.

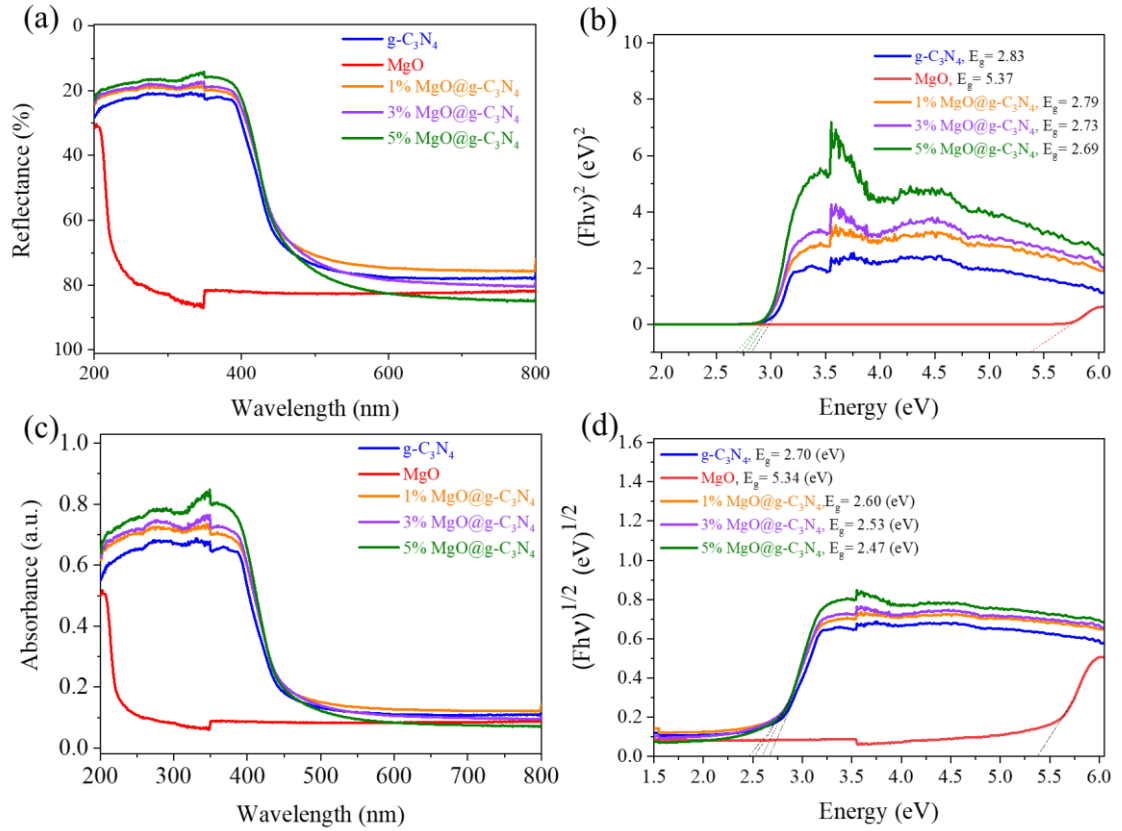


**Figure 9:** The DRS spectra reflectance (a), the direct band gap (b), the DRS spectra absorbance (c), and the indirect bandgap (d) of the materials.

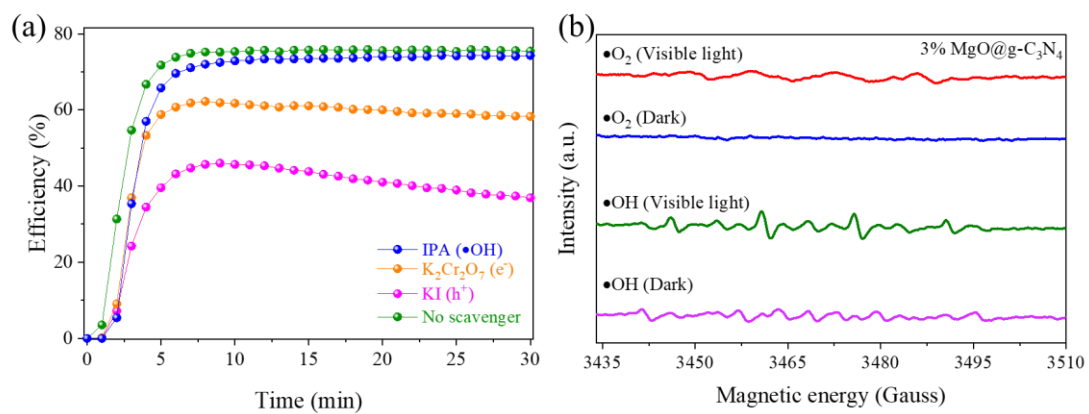


**Figure 10:** Trapping test results of the materials (a), and detection radicals by ESR (b) over 3% MgO@g-C<sub>3</sub>N<sub>4</sub>.

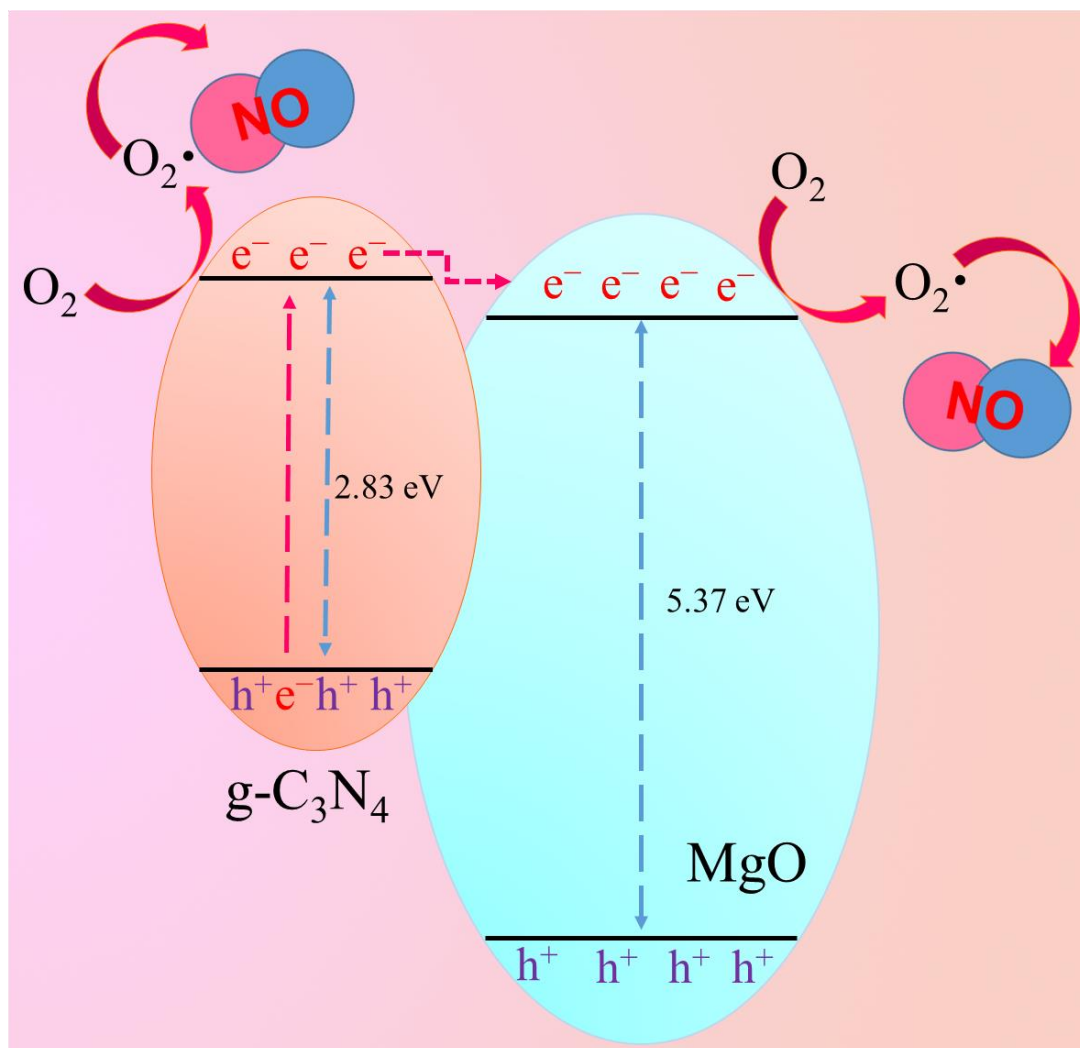


**Figure 11:** Proposed photocatalytic mechanism of materials.